ELSEVIER

Journal of Wind Engineering
and Industrial Aerodynamics 93 (2005) 891–904

JOURNAL OF wind engineering AND industrial aerodynamics

www.elsevier.com/locate/jweia

# Numerical simulation of the wind field around different building arrangements

Aishe Zhang[a,b,*], Cuilan Gao[a], Ling Zhang[b]

[a]*Department of Civil Engineering, Shandong Institute of Architecture and Engineering, Jinan, Shandong 250014, PR China*

[b]*Department of Mechanics, School of Civil Engineering and Mechanics, Xi'an Jiaotong University, Xi'an, Shaanxi 710049, PR China*

Received 10 June 2003; received in revised form 7 June 2005; accepted 8 September 2005
Available online 18 October 2005

**Abstract**

A numerical model with the RNG $\kappa-\varepsilon$ turbulence closure model and a pressure correction algorithm of SIMPLEC is used to examine three different building configuration effects on wind flow. Comparisons of computational results with experimental data have been carried out for the vertical velocity profiles at some measurement points. For the experimental study, the building arrangements were presented by 1:150 scale models and tested in a low-speed wind tunnel. It was found that the wind environment for two improved arrangements with lower interval-to-height ratio is better than that for the reference layout with higher aspect ratio in terms of the natural ventilation. The interference effect is more obvious for two improved arrangements than the reference one. The numerical results also show that changing wind direction from perpendicular to the building facades to a 45°-incidence angle has significant effect on the flow field for different configurations.


*Keywords:* Numerical simulation; Turbulence; Wind direction; Wind flow in urban area; Building configuration; Natural ventilation; Wind environment

*Corresponding author. Department of Mechanics, School of Civil Engineering and Mechanics, Xi'an Jiaotong University, Xi'an, Shaanxi 710049, PR China. Tel.: +86 29 2669082; fax: +86 29 3237910.
*E-mail address:* acclan@263.net (A. Zhang).

0167-6105/$ - see front matter 
doi:10.1016/j.jweia.2005.09.001

## 1. Introduction

The wind flow patterns in an urban area may strongly affect the dispersion of pollutants around the building, the efficiency of natural ventilation, the wind pressure distributions on buildings, and the wind comfort at the height of pedestrian level. The air flow is influenced by various factors, such as the geometry and arrangements of adjacent buildings, the upstream terrain conditions and wind directions [1,2]. For wind environmental improvements, the building arrangement is one of the important parameters to be considered by planners and designers. So it is worth to be investigated for a better understanding of the atmospheric processes which determine pedestrian comfort and air quality.

Traditionally, the analysis and evaluation of wind environment mainly depends on wind tunnel tests. Nowadays, numerical simulation (often called computational fluid dynamics, CFD) has been widely accepted owing to the advantage of the tremendous progress of computer capabilities in recent years, and the advances in numerical modeling. Especially, if optimization design is to be undertaken and the environmental impact of planned urban developments is to be assessed, the numerical modeling is preferred to wind tunnel experiments, as the tests are usually expensive, and often long time is needed, particularly in the case of additional test requirements with modified building and environmental configurations.

In the recent past, many numerical simulations concerning the urban wind fields have been carried out. Johnson and Hunter [3] performed numerical studies on urban canyon environment using $\kappa-\varepsilon$ formulation and made a preliminary comparison of wind tunnel results with numerical modeling values. Song and He [4] used large eddy simulation (LES) approach to compute and evaluate the pedestrian wind environment under different geometry and wind conditions. They concluded that the numerical model was accurate by comparing numerical results with a number of standard wind tunnel tests [5]. Their conclusion showed that the two methods had general agreement but the numerical simulation overestimated the concentration gradient with the canyon air space. He et al. [6] simulated and experimented the air flow distributions in a built-up area with regularly aligned blocks, and examined the possibility of practical use of the cyclic boundary conditions. Due to the complexity of the problem, the general rules are hard to be established and specific studies are needed for different building planning.

The objective of the present work is to apply the numerical simulation method to the wind flow around buildings for different configurations. Firstly, the wind environment of a referenced configuration is examined. Then two improved arrangement results are compared with those calculated in the referenced layout. For all these purposes, the unstructured grid system, the SIMPLEC method, and RNG $\kappa-\varepsilon$ turbulence model are adopted.

## 2. Scheme analysis

The area considered in this study is a residential zone in the South China. Fig. 1(a) (hereafter referred as Scheme I) shows a typical arrangement consisting of a group of simple rectangular prisms with the same height and width. The side length, $L_1$, (building Model 1) is two times $L_2$ (building Model 2). The aspect ratio of distance $B_1$, between the up- and down-stream rows, to the building height $H$ is set to 1.0. The interval, $B_2$, between

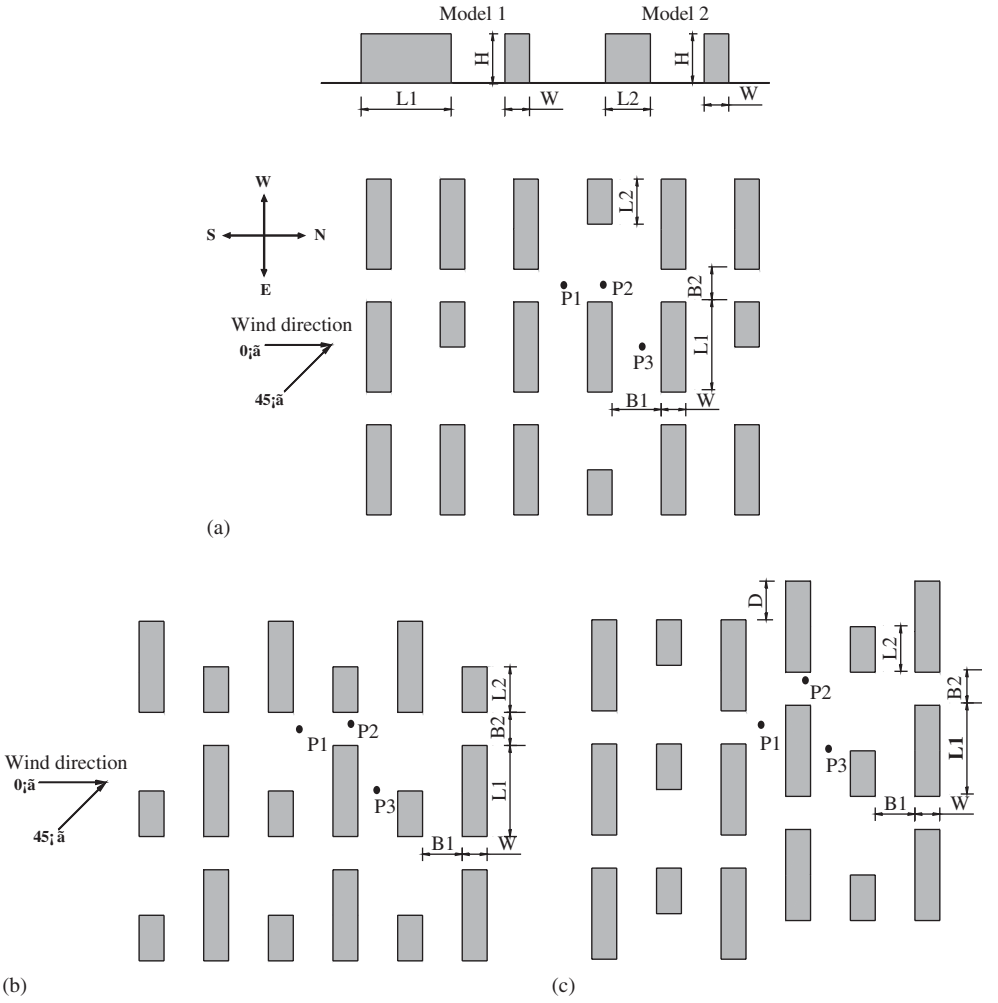


Fig. 1. Schematic diagram of different building configurations. ($H = 18$ m, $W = 9$ m, $L_1 = 48$ m, $L_2 = 24$ m): (a) referenced arrangement (Scheme I), (b) improved arrangement (Scheme II) and (c) improved arrangement (Scheme III).

adjacent two longer side buildings arranged side-by-side is $0.67H$. To comparing the building area density and the wind fields with those of the following layouts, the configuration in Scheme I is selected as the reference arrangement.

Figs. 1(b) and (c) (hereafter Schemes II and III, respectively) depict two different improved configurations (the distance $B_1$ is reduced), respectively. In these figures, the interval $B_1$ becomes $0.7H$, $B_2$ and $H$ are the same as those in Scheme I. In Fig. 1(c), the buildings are aligned in a staggered group and the distance **D** is set to 0.78 H. The parameters for different arrangements are listed in Table 1. The geometrical parameters describing the building configurations are as follows:

$$\text{Frontal aspect ratio}: \ \lambda_{\text{front}} = \left(\sum_{i=1}^{n} A_{i,\ \text{frontal area}}\right) \Big/ A_{\text{total}}, \tag{1}$$

Table 1
Parameters of building arrangement

| Case | $B_1/H$ | $B_2/H$ | $D/H$ | $\lambda_{front}$ | $\lambda_{area}$ |
|---|---|---|---|---|---|
| Scheme I | 1.0 | 0.67 | 0.0 | 0.376 | 0.188 |
| Scheme II | 0.7 | 0.67 | 0.0 | 0.397 | 0.198 |
| Scheme III | 0.7 | 0.67 | 0.78 | 0.404 | 0.202 |

$$\text{Plan area density}: \ \lambda_{area} = \left(\sum_{i=1}^{n} B_i L_i\right) \Big/ A_{total}. \tag{2}$$

where $n$ is the number of buildings, $A_{i,\text{ frontal area}}$ is the frontal building area normal to the wind of each one, $B_i$ and $L_i$ is the building width and length, respectively. $A_{total}$ is the total plan area.

Wind records performed in this area over 10 years indicate that the strongest wind direction in the summer is South wind (hereafter referred as S–N), followed by Southeast wind (hereafter referred as SE–NW) [7]. Assuming the same directions prevail for the building arrangement presented in this paper, the S–N and SE–NW wind directions are to be considered for the wind field studies.

The experiments with 1:150 scale models were carried out in a low-speed wind tunnel at the Hunan University, Hunan, China. The experiments were performed only for the prevailing S–N wind direction. Some of the tested points are shown in Fig. 1 where the vertical profiles were measured using seven-hole probes. For further details of the experiment, see Ref. [8]. The experiments were used to verify the performance of the numerical simulation for these complicated configurations.

## 3. Numerical simulation

The governing equations of incompressible turbulent wind flow around buildings are continuity and the Reynolds-averaged Navier–Stokes equations, expressed as follows:

$$\frac{\partial u_i}{\partial x_i} = 0, \tag{3}$$

$$\frac{\partial}{\partial x_j}(\rho u_j u_i) = -\frac{\partial p}{\partial x_i} + \frac{\partial}{\partial x_j}\left[\mu\left(\frac{\partial u_i}{\partial x_j} + \frac{\partial u_j}{\partial x_i}\right) - \rho\overline{u'_i u'_j}\right]. \tag{4}$$

To model the turbulent flow, the RNG $\kappa-\varepsilon$ model [9] is adopted here for computational efficiency and accuracy. The model differs from the standard $\kappa-\varepsilon$ model [10] only through the modification to the equation for $\varepsilon$. The RNG $\kappa-\varepsilon$ model is expressed by the following equations:

$$-\rho\overline{u'_i u'_j} = \mu_t\left(\frac{\partial u_i}{\partial x_j} + \frac{\partial u_j}{\partial x_i}\right) - \frac{2}{3}\delta_{ij}\rho k, \tag{5}$$

$$\frac{\partial}{\partial x_j}(\rho u_j k) = \frac{\partial}{\partial x_j}\left[\left(\mu + \frac{\mu_t}{\sigma_k}\right)\frac{\partial k}{\partial x_j}\right] + \mu_t\left(\frac{\partial u_i}{\partial x_j} + \frac{\partial u_j}{\partial x_i}\right)\frac{\partial u_i}{\partial x_j} - \rho\varepsilon, \tag{6}$$

Table 2
Turbulence model constant values

| Constant | $C_\mu$ | $\sigma_\kappa$ | $\sigma_\varepsilon$ | $C_2$ | $\eta_0$ | $\beta$ |
|---|---|---|---|---|---|---|
| Value | 0.085 | 0.7179 | 0.7179 | 1.68 | 4.38 | 0.015 |

$$\frac{\partial}{\partial x_j}(\rho u_j \varepsilon) = \frac{\partial}{\partial x_j}\left[\left(\mu + \frac{\mu_t}{\sigma_\varepsilon}\right)\frac{\partial \varepsilon}{\partial x_j}\right] + C_1 \frac{\varepsilon}{k}\,\mu_t\left(\frac{\partial u_i}{\partial x_j} + \frac{\partial u_j}{\partial x_i}\right)\frac{\partial u_i}{\partial x_j} - C_2 \rho \frac{\varepsilon^2}{k}, \tag{7}$$

where

$$k = \frac{1}{2}\overline{u'_i u'_j},\quad \varepsilon = \mu\overline{\left(\frac{\partial u'_i}{\partial x_j}\right)\left(\frac{\partial u'_j}{\partial x_i}\right)},\quad \mu_t = C_\mu \frac{\rho k^2}{\varepsilon}, \tag{8}$$

$$C_1 = 1.42 - \eta\,\frac{1-\eta/\eta_0}{1+\beta\eta^3}, \tag{9}$$

$$\eta = Sk/\varepsilon,\ S = (2S_{ij}S_{ij})^{1/2}, \tag{10}$$

$$S_{ij} = \frac{1}{2}\left(\frac{\partial u_i}{\partial x_j} + \frac{\partial u_j}{\partial x_i}\right). \tag{11}$$

In the above equations, $u_i$ and $u'_i$ are the mean and turbulent fluctuating velocity components in the $x_i$ direction, respectively. $p$ is the mean pressure and $\rho$ is the fluid density. $k$ and $\varepsilon$ stand for the turbulence kinetic energy and its rate of dissipation, respectively. $\mu$ and $\mu_t$ are the molecular and eddy viscosity, respectively. $\sigma_k$, $\sigma_\varepsilon$, $C_\mu$, $C_2$, $\eta_0$ and $\beta$ are the turbulence model constants tabulated in Table 2.

The inlet boundary conditions are presented as follows:

$$\frac{u}{U_0} = \left(\frac{z}{z_0}\right)^\alpha, \tag{12}$$

$$\kappa = \frac{3}{2}(ui_t)^2, \tag{13}$$

$$\varepsilon = C_\mu k^{3/2}/l \tag{14}$$

in the above equations, $u$ is the horizontal wind speed at elevation $z$, $U_0$ is the speed at the reference elevation $z_0$, $\alpha$ is the parameter that varies with ground roughness, $i_t$ is the turbulence intensity, $l$ is the characteristic length [11]. All of these parameters are measured in the wind tunnel test. The undisturbed streamwise velocity and the turbulence intensity are shown in Fig. 2. The reference velocity $u_0$ is set to be 4.5 m/s at the elevation $z_0 = 10$ m. In order to compare the numerical results with the experimental quantities, the exponent $\alpha$ is selected as 0.22 obtained from the experiment [7].

At the upper boundary, the full-slip velocity condition is adopted. Confirming the overall mass conservation through the flow domain by correcting the outlet velocity components are used as the outlet boundary conditions.

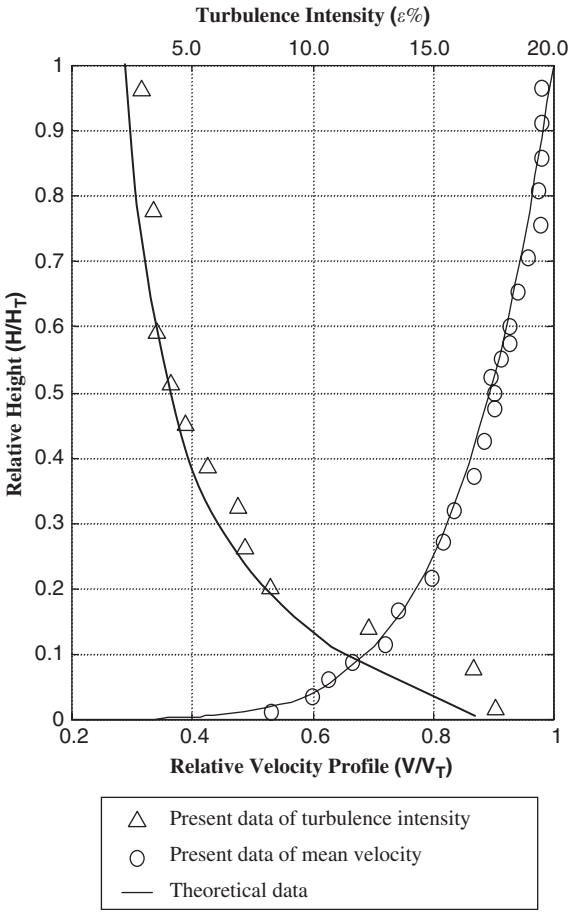


Fig. 2. Mean velocity and turbulence intensity profile.

At the ground wall boundary, the wall function method is adopted here. The boundary conditions are as follows:

$$u^+ = \frac{u_\tau}{\kappa} \ln(E y_w^+), \tag{15}$$

$$k_w = u_\tau^2 / \sqrt{C_\mu}, \tag{16}$$

$$\varepsilon = \frac{C_\mu^{3/4} k_w^{3/2}}{\kappa y_w}, \tag{17}$$

$$\tau_w = \kappa \rho C_\mu^{1/4} k^{1/2} \Big/ \ln(E y_w^+), \tag{18}$$

where $y_w^+$, $\kappa$ and $E$ are the wall coordinates, the von Karman constant and a constant, respectively, usually $\kappa = 0.40-0.42$, $E = 0.22$. The wall coordinate $y_w^+$ is defined as $y_w^+ = \rho u_\tau y_w/\mu$, and $u_\tau = \sqrt{\tau_w/\rho}$. The dimensionless distance $y_w^+$ should be in the wall

coordinate range:

$$11.5-30 \leqslant y_w^+ \leqslant 200-400$$

to satisfy the velocity log law [10].

The finite volume method [12] is chosen for the discretization of the equations on an unstructured grid system. Smaller grid size is used near the buildings and the ground. The control equations are solved by pressure correction procedure of SIMPLEC method [13]. The finite discretization in this study is based on a collocated-grid definition of the variables. All dependent variables are stored at the same location in the integration domain. The momentum interpolation method (MIM)[14] is adopted to remove the oscillating problems, which might otherwise arise from the collocated grids. The QUICK [15] scheme is used for discretization of convective terms to reduce the numerical diffusion of the difference scheme. Second-order central difference is used for the discretization of diffusion terms. An iterative procedure is used for the solution of the discretization equations. The finite difference linear equations (inner iteration) are solved by Strong Implicit Procedure (SIP) [16]. Computations are terminated when the initial residual in 2-norm is reduced by a factor of $10^6$. Then the pressure and velocity distributions are obtained.

## 4. Results and discussion

In this section, the velocity fields around the buildings for all the schemes are presented. The experimental results were obtained only in the S–N wind direction.

Figs. 3(a) and (b) show the vertical profile variations of the velocity magnitude at different points as shown in Fig. 1 for S–N and SE–NW wind directions, respectively. To evaluate the changes in the local wind field conditions, the velocities are converted into the dimensionless velocity ratios by dividing the reference velocity $U_0$ that is the velocity at the reference height. In Fig. 3(a), the numerical predictions overall are in satisfactory agreement with the experimental results, but the major discrepancies are present at about the roof and lower levels. This difference could be attributed to the fact that these measurement points are in location of highly complex recirculating flow regions. Neither experimental nor computed data are considered accurate in these locations. The experimental errors are due to measuring device limitations. The computational errors mainly include the inaccuracies introduced by the discretization scheme, parameter selection, and algebraic equation solutions.

The results shown in Figs. 3(a) and (b) also indicate that the vertical profile of velocity is affected by the wind direction. The velocities for the SE–NW wind are greater than that for the S–N wind direction, particularly for P3.

In Figs. 4 and 5, the similar comparisons of numerical predictions with the experimental results for Schemes II and III in the two wind directions are shown, respectively. Some discrepancies can be observed about the roof level. In general, however, the overall agreement between numerical predictions and experimental measurements is good. It can be seen that, for the aspect ratio, $B_1/H$, of 0.7, the vertical normalized wind velocity for P2 was reduced for Scheme III (staggered building configuration) as compared to Scheme II (“regular” building configuration) for both the S–N and SE–NW wind directions, although the wind velocity was a little changed for P1 and P3. These are some qualitative

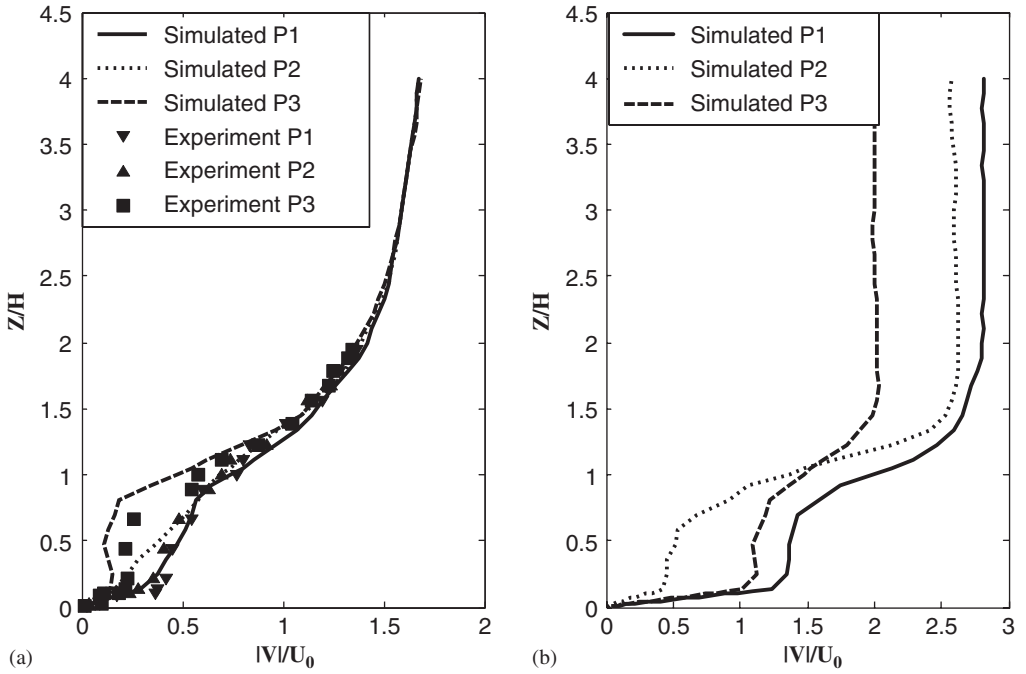


Fig. 3. Experimental and numerical normalized wind velocity profiles for Scheme I: (a) S–N wind and (b) SE–NW wind.

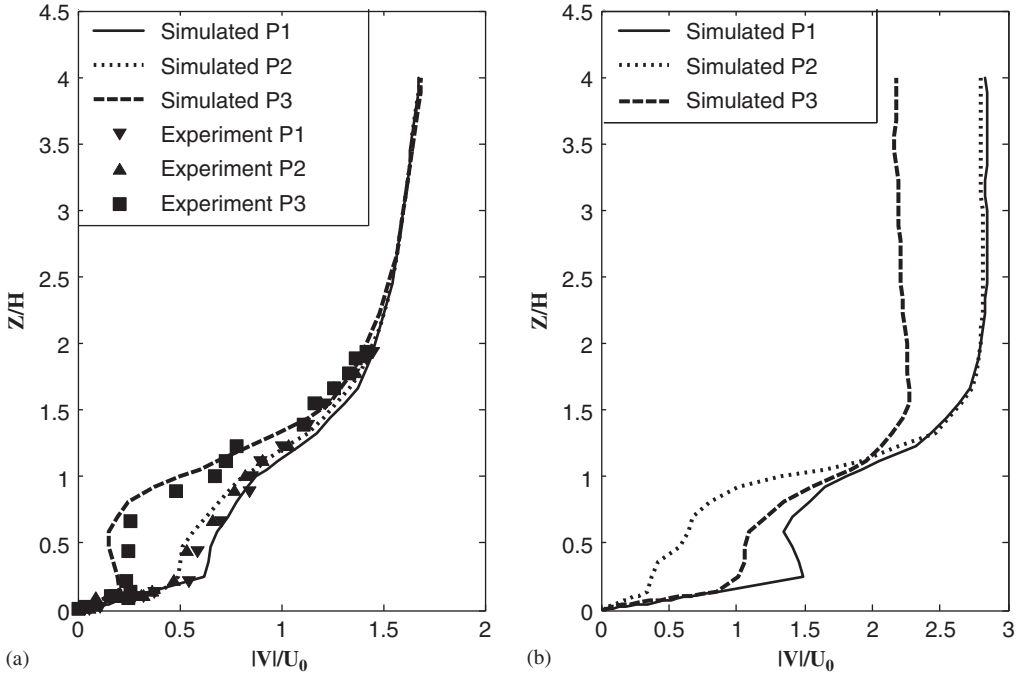


Fig. 4. Experimental and numerical normalized wind velocity profiles for Scheme II: (a) S–N wind and (b) SE–NW wind.

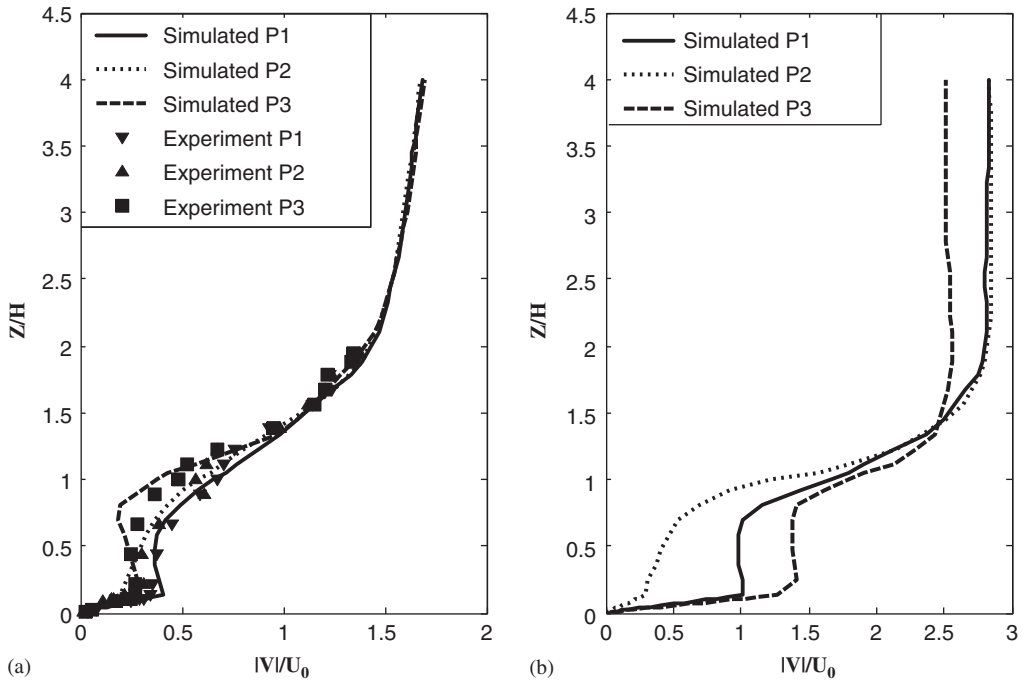


Fig. 5. Experimental and numerical normalized wind velocity profiles for Scheme III: (a) S–N wind and (b) SE–NW wind.

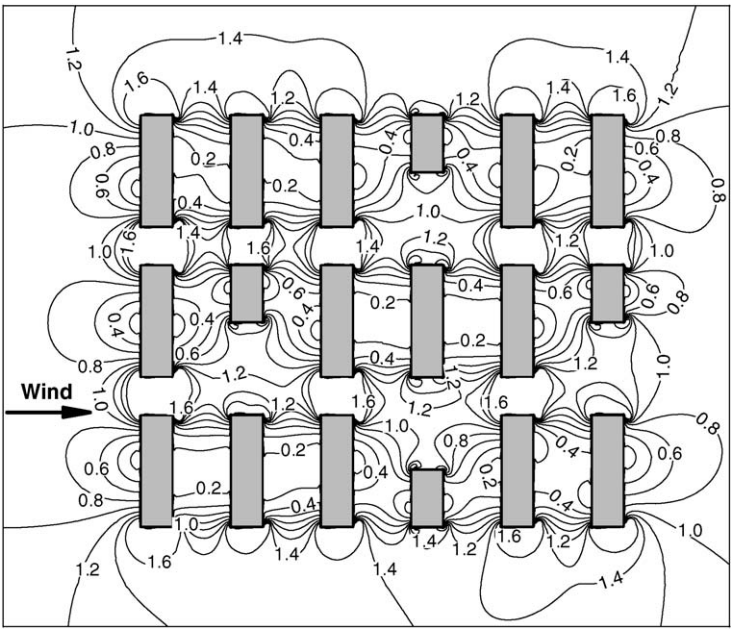


Fig. 6. Computed normalized velocity field around the buildings of Scheme I at 2 m from the ground level for S–N wind direction.

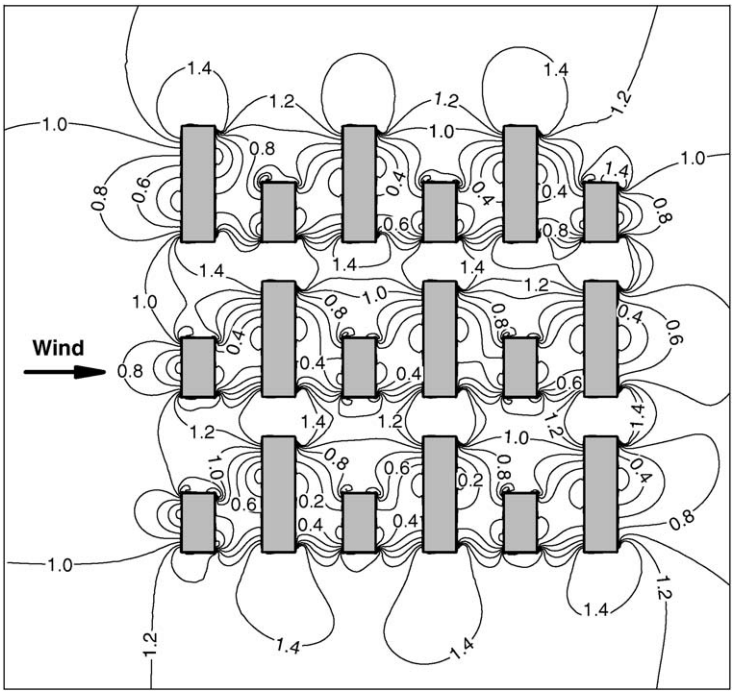


Fig. 7. Computed normalized velocity field around the buildings of Scheme II at 2 m from the ground level for S–N wind direction.

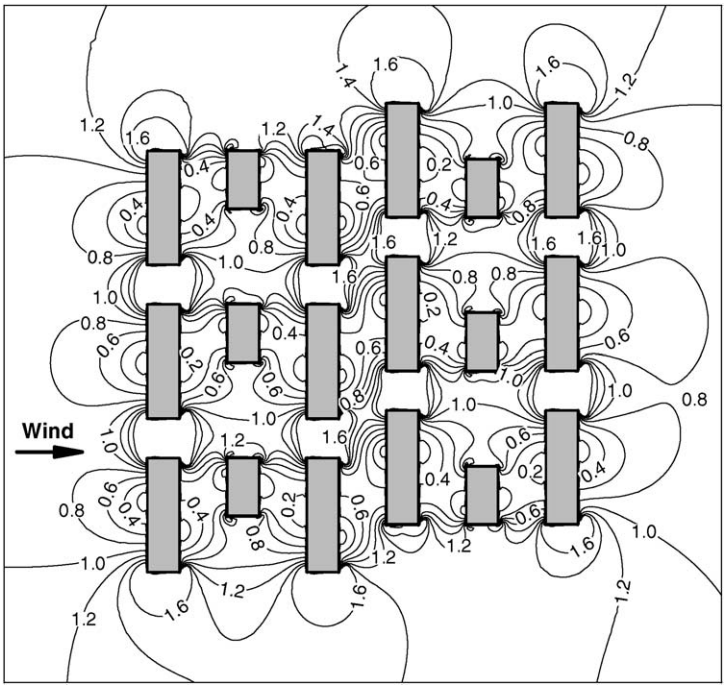


Fig. 8. Computed normalized velocity field around the buildings of Scheme III at 2 m from the ground level for S–N wind direction.

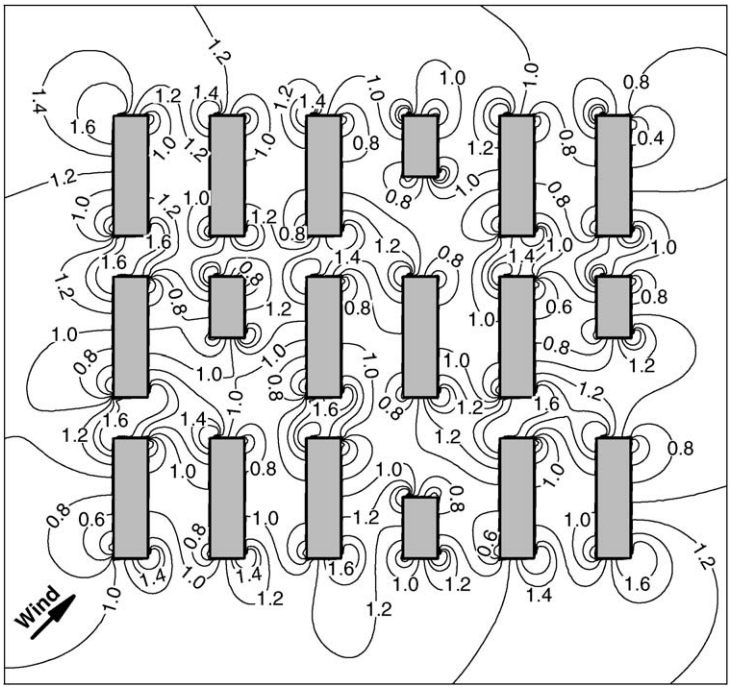


Fig. 9. Computed normalized velocity field around the buildings of Scheme I at the level of 2 m from the ground for SE–NW wind direction.

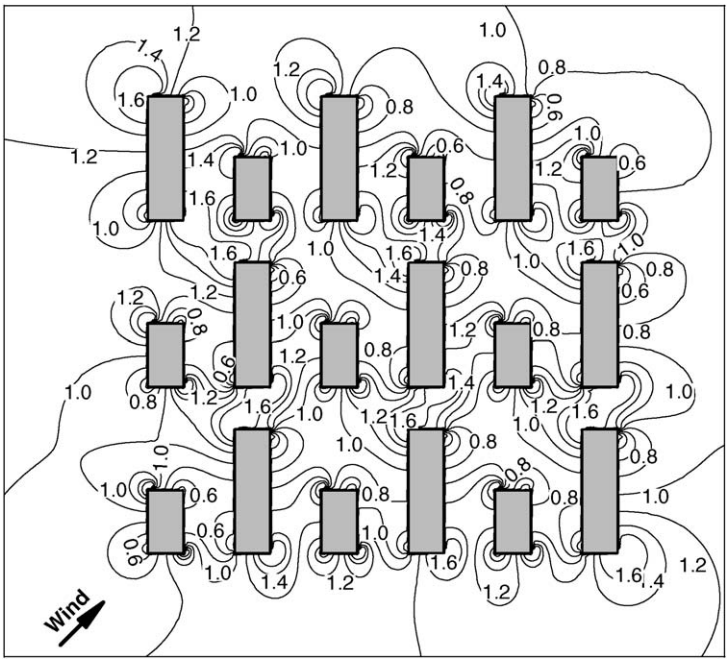


Fig. 10. Computed normalized velocity field around the buildings of Scheme II at the level of 2 m from the ground for SE–NW wind direction.

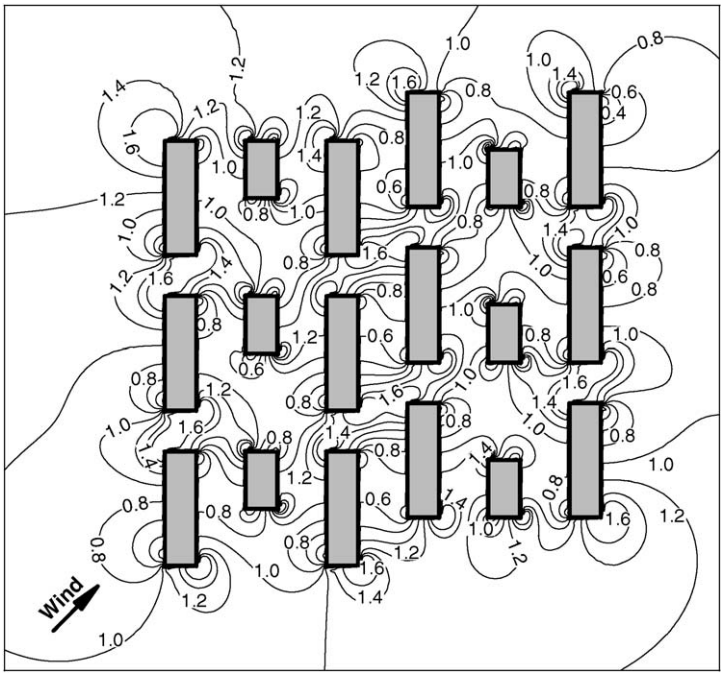


Fig. 11. Computed normalized velocity field around the buildings of Scheme III at the level of 2 m from the ground for SE–NW wind direction.

conclusions. However, the effect of different arrangement on wind field is still to be further analyzed.

Figs. 6–8 show the normalized velocity fields at the pedestrian level of 2 m from the ground for Schemes I, II and III, respectively, for the S–N wind direction. As the wind blows against the broad sides of buildings, it generates very large and strong horseshoe vortices. This is the reason why the wind in front of the buildings at the pedestrian level blows downward and away from the buildings. In the above three figures, it is impossible to obtain these detailed velocity fields with the wind tunnel test owing to measuring device limitations.

By integrating the velocity field over all the alleyways' area, an increase of 25.6% for the general velocity for Scheme II is produced as compared to that for Scheme I, but about a reduction of 7.9% is obtained in comparison with the velocity for Scheme III.

For the SE–NW wind direction, the velocity fields at 2 m level above the ground for Schemes I, II and III are shown in Figs. 9–11, respectively, which depict the effect of wind direction on the velocity distribution. By integrating the velocity over all the alleyways' area, the increase of 132.3% for Scheme I, 112.8% for Scheme II, and 100.9% for Scheme III in this wind direction as compared to the corresponding situations for the S–N wind are produced. For the SE–NW wind, the overall velocity magnitude increase of 13.7% and 3.8% for the overall velocity for Scheme III by comparison with Schemes I and II, respectively, are obtained.

In the summer, the S–N and SE–NW wind prevails on the site. By comparing Figs. 6–11, it can be seen that the staggered group arrangement (Scheme III) helps to introduce more

wind into the site in the two wind directions. Therefore, Scheme III can provide a good wind environment and potential to use natural ventilation.

## 5. Conclusion

A numerical simulation for evaluating the wind field under different building arrangements and wind conditions is presented in this paper. Computational results are generally in good agreement with the experimental data for the locations experimentally tested. The results also show that the numerical method is a relatively more economical and faster tool to evaluate the wind environment.

By comparing different building schemes, it is found that the wind field depends strongly on the building layout and the wind direction. Scheme III (the staggered group arrangement) helps to introduce more wind into the site in the two wind directions for S–N and SE–NW wind directions. Consequently, Scheme III can provide a good wind environment and potential to use natural ventilation.

In order to make use of the advantage of the computational model, this type of the research is desirable during the project design phase. If necessary, the building arrangement would be improved.

## Acknowledgements

This work was financially supported by the Doctoral Foundation of Xi'an Jiaotong University, China. The helpful assistance of Dr. Litsiang Kang in computing aspects is also acknowledged with thanks.

## References

[1] B.E. Lee, M. Hussain, B. Soliman, Prediction natural ventilation forces upon low-rise buildings, ASHRAE J. 22 (1980) 35–39.
[2] A.C. Khanduri, T. Stathopoulos, C. Bédard, Wind-induced interference effects on buildings—a review of the state-of-the-art, Eng. Struct. 20 (1998) 617–630.
[3] G.T. Johnson, L.J. Hunter, Urban wind flows: wind tunnel and numerical simulations—a preliminary comparison, Env. Model. Softw. Environ. Data News 13 (1998) 279–286.
[4] C.C. Song, J. He, Evaluation of pedestrian winds in urban area by numerical approach, J. Wind Eng. Ind. Aerodyn. 81 (1999) 295–309.
[5] J. He, C.C. Song, A numerical simulation of wind flow around the TTU building and the roof corner vortex, J. Wind Eng. Ind. Aerodyn. 67&68 (1997) 547–558.
[6] P. He, T. Katayama, T. Hayashi, J. Tsutsumi, J. Tanimoto, L. Hosooka, Numerical simulation of air flow in an urban with regularly aligned blocks, J. Wind Eng. Ind. Aerodyn. 67&68 (1997) 281–291.
[7] Guangdong Construction Meteorological Parameter Standards (DBJ15-1-90), (in Chinese).
[8] Z.Q. Wang, Multi-storey building arrangement and its natural ventilation in South China, South Architechture 77 (1996) 54–60 (in Chinese).
[9] V. Yakhot, S.A. Orszag, S. Thangam, T.B. Gatski, C.G. Speziale, Development of turbulence models for shear flows by a double expansion technique, Phys. Fluids A 4 (7) (1992) 1510–1520.
[10] B.E. Launder, D.E. Spalding, The numerical computation of turbulent flows, Comp. Meth. Appl. Mech. Eng. 3 (1974) 269–289.
[11] E. Simiu, R.H. Scanlan, Wind Effects on Structures: An Introduction to Wind Engineering, Wiley, New York, 1992.
[12] S.V. Patanker, Numerical Heat Transfer and Fluid Flow, McGraw-Hill, New York, 1990.
[13] J.P. Van Doormal, G.D. Raithby, Enhancement of the SIMPLE method for predicting incompressible fluid flow, Numer. Heat Transfer 7 (1984) 147–163.

[14] C.M. Rhie, W.L. Chow, A numerical study of the turbulent flow past an isolated airfoil with trailing edge separation, AIAA J. 21 (1983) 1525–1552.
[15] B.P. Leonard, A stable and accurate convective modeling procedure based on quadratic upstream interpolation, Comput. Meth. Appl. Mech. Eng. 19 (1979) 59–98.
[16] T. Tamura, H. Kawai, S. Kawamoto, K. Nozawa, S. Sakamoto, T. Ohkuma, Numerical prediction of wind loading on buildings and structures—activities of AIJ cooperative project on CFD, J. Wind Eng. Ind. Aerodyn. 67&68 (1997) 671–685.